

# Asymptotic formulae for flow in superhydrophobic channels with longitudinal ridges and protruding menisci

Toby L. Kirk

*Department of Mathematics, Imperial College London, London SW7 2AZ, UK*

## Abstract

This paper presents new analytical formulae for flow in a channel with one or both walls patterned with a longitudinal array of ridges and arbitrarily protruding menisci. Derived from a matched asymptotic expansion, they extend results by Crowdy (*J. Fluid Mech.*, vol. 791, 2016, R7) for shear flow, and thus make no restriction on the protrusion into or out of the liquid. The slip length formula is compared against full numerical solutions and, despite the assumption of small ridge period in its derivation, is found to have a very large range of validity; relative errors are small even for periods large enough for the protruding menisci to degrade the flow and touch the opposing wall.

## 1 Introduction

Superhydrophobic surfaces have received considerable attention in recent years due to their low wettability and reduced viscous drag [Ou et al., 2004]. Typically they consist of a no-slip surface patterned with micrometer structures such as pillars or grooves. A liquid in the Cassie state—where gas is trapped in the micro-cavities—experiences low shear-stress on the liquid-gas interfaces (menisci) and a reduced overall viscous drag, frequently measured in terms of an apparent slip length. Flows over many different superhydrophobic microstructure geometries have been studied extensively, with experiments, numerical solutions, and analytical techniques [Ou et al., 2004, Ou and Rothstein, 2005, Lauga and Stone, 2003, Davies et al., 2006, Cottin-Bizonne et al., 2004].

An important class of surfaces is a parallel array of ridges aligned with the flow direction, owing to their advantage in heat transfer performance compared to pillars [Enright et al., 2014], and advantage in drag reduction compared to transverse (oriented perpendicular to the flow direction) ridges [Teo and Khoo, 2009]. The particular geometry of the structures, and the interfaces that span them, have a great effect on the resulting drag reduction. Most initial analytical and computational studies assumed that the menisci are flat for simplicity, but they can be highly curved due to the high pressure gradients required in experiments [Ou and Rothstein, 2005]. Experiments for transverse ridges by Steinberger et al. [2007] showed that the slip length can become negative, indicating flow degradation, if the

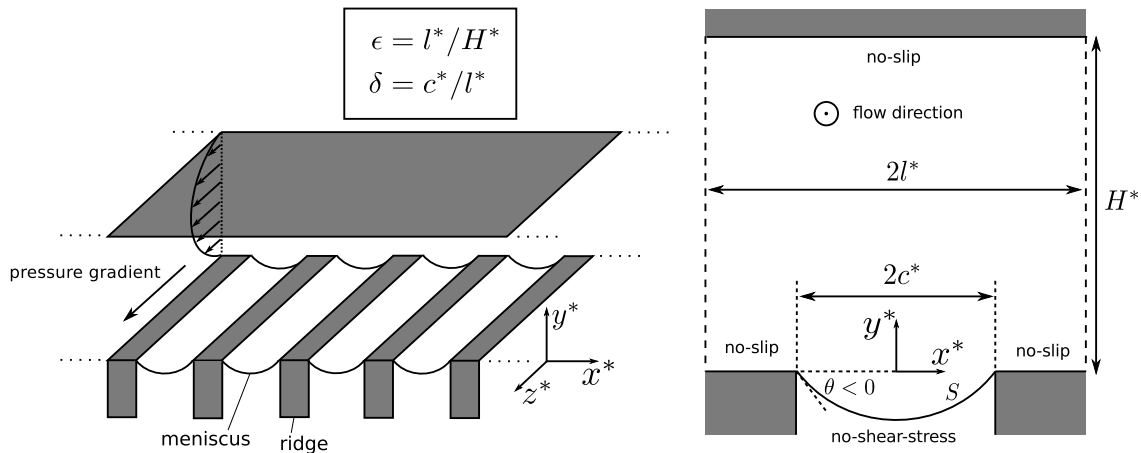


Figure 1.1: Schematic of the pressure-driven channel flow aligned with a periodic array of ridges, period  $2l^*$ , and groove width  $2c^*$ . Circular-cross-section menisci contact the ridge corner at angle  $\theta$  (with  $\theta < 0$  corresponding to downward protrusion). The distance from ridge tips to the opposing wall is  $H^*$ .

meniscus protrusion into the liquid is too large. This motivated Davis and Lauga [2009] to develop an analytical model for shear-flow over transverse ridges, confirming this dependence on curvature. Crowdy [2010] extended the model to shear flow over longitudinal ridges, where the slip length remains positive but with a considerable dependence on the protrusion angle. These studies made the so-called dilute approximation, i.e., that the menisci were spaced widely apart, which was recently extended to higher order accuracy [Crowdy, 2016]. The opposing limit of densely packed menisci (small solid fraction) was considered by Schnitzer [2017]. Also in this limit, Ybert et al. [2007] found slip length scaling laws consistent with their numerical results, and captured the often neglected effects of molecular slip, and shear-stress exerted by the gas. On the other hand, Ng and Wang [2011] performed numerical solutions for any spacing, and also considered 3D shear flows over spherical menisci.

When the parallel ridges are taken to pattern one or both walls of a channel or pipe, only numerical or experimental studies have been able to account for significant meniscus curvature. Sbragaglia and Prosperetti [2007] considered a channel (and Wang et al. [2014] a pipe) with longitudinal ridges on one wall and accounted for small meniscus curvature using boundary perturbation. They found analytical formulae only for an infinite channel thickness, and Kirk et al. [2017] extended these formulae to ridges on both walls, but included all higher order corrections. When the curvature is not small, which is true for applications involving liquid metals [Lam et al., 2015], a detailed study for longitudinal ridges on one channel wall was conducted by Teo and Khoo [2010] using a finite-element method. They assessed the accuracy of the boundary perturbation, but also showed that the slip length can become negative for large protrusion, as for transverse ridges, when channel thicknesses are low enough—behaviour not predicted by the formulae for shear flows in the previous paragraph.

In analysing flows over parallel ridges, many asymptotic limits of geometric length scales have been employed. Neglecting the gas phase, consider a channel of height  $H^*$  with parallel ridges of period  $2l^*$  and cavity width  $2c^*$  patterning one wall, as in figure 1.1, or both walls symmetrically. (Asterisks denote dimensional quantities.) The pressure difference between the liquid and gas causes the menisci to form circular arcs, protruding into or out of the cavities. There are three length ratios that describe the geometry: (i)  $\epsilon = l^*/H^*$ , the ratio of ridge period to channel height; (ii)  $\delta = c^*/l^*$ , the slip fraction or ratio of groove width to ridge period; (iii)  $\theta$ , the protrusion angle that the meniscus makes with the horizontal at the corners of the ridges ( $\theta > 0$  corresponds to protrusion into the liquid).

Sbragaglia and Prosperetti [2007] considered  $|\theta| \ll 1$ , with no restriction on  $\epsilon$  or  $\delta$ , however their analytical results were only for an unbounded shear-flow, corresponding to  $\epsilon = 0$ . The dilute [Davis and Lauga, 2009, Crowdy, 2010, 2016] and dense [Schnitzer, 2017] meniscus packing assumptions correspond to  $\delta \ll 1$  and  $1 - \delta \ll 1$ , respectively, but previous work is only for  $\epsilon = 0$ . The lack of analytical models for curvature in channels ( $\epsilon, \theta \neq 0$ ) makes tasks such as channel design and optimisation difficult and time consuming. Consequently, the slip length formulae for unbounded flows ( $\epsilon = 0$ ) are often used for channel flows far outside their validity if the menisci are curved [Maynes and Crockett, 2014, Maynes et al., 2013, 2008, Enright et al., 2014].

In this paper we present solutions for flow in a channel with longitudinal ridges on one or both walls for finite channel heights, i.e.,  $\epsilon \neq 0$ , that are valid for any protrusion angle  $\theta$ , and extend the shear-flow solutions of Crowdy [2016]. We consider the limit of small period to height ratio,  $\epsilon \ll 1$ , using matched asymptotic expansions as per Hodes et al. [2017], who considered a flat meniscus. Two of Crowdy's approximations for the nondimensional shear-flow slip length  $\lambda = \lambda^*/l^*$  are

$$\lambda_0 = \delta^2 \frac{3\pi^3 - 4\pi^2\theta + 2\pi\theta^2}{12(\pi - \theta)^2}, \quad \lambda_1 = \frac{\lambda_0}{1 - \frac{\pi}{6}\lambda_0}, \quad (1.1)$$

with  $\lambda_1$  a higher order approximation than  $\lambda_0$ . The nondimensional slip length for a channel with ridges on one wall and a smooth no-slip surface on the other, is denoted  $\beta = \beta^*/H^*$ , to distinguish it from  $\lambda$ . It is defined as the effective slip length that realises the same flow rate per period as the actual flow. The main result of this paper is an extension of  $\lambda_1$  to the formula

$$\beta = \frac{\epsilon\lambda_1 - \epsilon^2\delta^3 I(1 + \frac{\pi}{6}\lambda_1) [2 + (\epsilon^2 - \frac{\pi}{6}\epsilon)\delta^3 I] + (1 + \epsilon\lambda_1)\epsilon^3\delta^4(F - G)}{1 + \epsilon^2\delta^3 I(1 + \frac{\pi}{6}\lambda_1) [2 + (\epsilon^2 - \frac{\pi}{6}\epsilon)\delta^3 I] - (1 + \epsilon\lambda_1)\epsilon^3\delta^4(F - G)}, \quad (1.2)$$

where

$$I(\theta) = 16 \sin \theta \int_0^{\pi/2} \frac{\tan^{2\alpha} \phi [\cos \theta \tan^{2\alpha} \phi + 2 \tan^\alpha \phi + \cos \theta] d\phi}{[\tan^{2\alpha} \phi + 2 \cos \theta \tan^\alpha \phi + 1]^3}, \quad \alpha = \frac{2}{\pi}(\pi - \theta), \quad (1.3)$$

$$F(\theta) = \csc^4 \theta \left[ \theta (3 + 2 \cos 2\theta) - \frac{7}{3} \sin 2\theta - \frac{1}{12} \sin 4\theta \right], \quad (1.4)$$

and  $G(\theta)$  is given up to quadrature by (5.7), or by the correlation (5.11). The result for a similar channel with longitudinal ridges on both walls is simpler, but given in terms of the same functions,

$$\beta^{(sym)} = \epsilon\lambda_1 - \epsilon^2\delta^3 I \left(1 + \frac{\pi}{6}\lambda_1\right) \left(2 - \frac{\pi}{6}\epsilon\delta^3 I\right) + \epsilon^3\delta^4(F - G). \quad (1.5)$$

Formulae (1.2) and (1.5) elucidate the differences between the shear-flow and channel flow slip lengths when the menisci are curved. They are explicit and valid for the entire range of protrusion angles  $\theta \in [-\pi/2, \pi/2]$ , and a very large range of  $\epsilon$ . Formula (1.2) is compared against finite element computations and the accuracy in  $\delta$  is similar to that of  $\lambda_1$ : up to  $\epsilon = 0.5$ , the maximum relative error for  $\delta = 0.5$  and  $0.75$  is  $\sim 0.8\%$  and  $\sim 8\%$ , respectively. This accuracy holds even up to  $\epsilon = 2.5$ , where the meniscus can touch the opposite wall and  $\beta$  becomes negative, as seen by Teo and Khoo [2010].

The matched asymptotics procedure for  $\epsilon \ll 1$  reduces the problem to a shear flow in an inner region near the ridges with a forcing on the meniscus, the solution of which gives an exponentially accurate solution for the channel flow. We only consider the dilute limit  $\delta \ll 1$  of this inner problem, but the asymptotic decomposition holds for any periodic structuring, and can be extended to other limits or to include other physical effects.

## 2 Governing equations

We will focus on steady, fully-developed flow in a parallel plate channel with longitudinal ridges on one wall, as in figure 1.1. The analysis for the case of longitudinal ridges on both channel walls is almost identical, and can be found in the Supplementary Material. The flow is assumed unidirectional,  $\mathbf{u}^* = (0, 0, w^*(x^*, y^*))$ , governed by  $\mu\nabla^2 w^* = \partial p^*/\partial z^*$  in the cross-plane, with a constant pressure gradient  $-\partial p^*/\partial z^*$  and viscosity  $\mu$ . We need only consider one period window,  $x^* \in [-l^*, l^*]$ , with a cavity located at  $x^* \in [-c^*, c^*]$ . The gas phase and streamwise curvature variation are neglected. The nondimensional velocity and lengths are defined as  $w = -(2\mu/H^{*2})(\partial p^*/\partial z^*)^{-1}w^*$  and  $(x, y) = (x^*, y^*)/H^*$ , giving the following nondimensional problem in the cross-plane,

$$\nabla^2 w = -2, \quad (2.1)$$

where  $\nabla^2 = \partial^2/\partial x^2 + \partial^2/\partial y^2$ , with no-slip at the top of the domain,

$$w = 0, \quad \text{on } y = 1, x \in [-\epsilon, \epsilon] \quad (2.2)$$

and mixed no-slip/no-shear-stress conditions at the bottom of the domain,

$$w = 0, \quad \text{on } y = 0, x \notin [-\epsilon\delta, \epsilon\delta] \quad (2.3)$$

$$\mathbf{n} \cdot \nabla w = 0, \quad \text{on the meniscus } S \quad (2.4)$$

where  $\mathbf{n}$  is the unit normal pointing into the liquid. Periodic or symmetry boundary conditions, i.e.,  $\partial w/\partial x = 0$ , apply at  $x = \pm\epsilon$ .

### 3 The limit of large channel height to ridge period, $\epsilon \ll 1$

The procedure of the matched asymptotic expansion for  $\epsilon = l^*/H^* \ll 1$  is similar to that in Hodes et al. [2017], to which we refer the reader for a more detailed description. In the limit  $\epsilon \rightarrow 0$ , the domain decomposes into an outer region where  $y = O(1)$  and the flow is 1D and parabolic, and an inner region near the ridges where  $y = O(\epsilon)$  and the  $x$  variation is present.

#### 3.1 Outer region: $y = O(1)$

After rescaling the transverse coordinate,  $X = x/\epsilon$ , and substituting a regular asymptotic expansion  $w \sim w_0 + \epsilon w_1 + \dots = \sum_{n=0}^{\infty} \epsilon^n w_n$  with  $X, y, w_n = O(1)$  into (2.1) and applying periodicity at each order, Hodes *et al.* showed that each  $w_n$  is only a function of  $y$ , i.e.,  $w_n = w_n(y)$  for all  $n \geq 0$ . This means  $w$  is independent of  $X$  in the outer region to all algebraic orders in  $\epsilon$ . Integrating at each order and applying only the condition (2.2) at  $y = 1$  gives the one dimensional outer solution

$$w = -y^2 + y + B(\epsilon)(1 - y), \quad (3.1)$$

where  $B(\epsilon)$  is the (asymptotic) series  $B(\epsilon) := \sum_{n \geq 0} B_n \epsilon^n$  and the  $B_n$  are  $O(1)$  constants.

The mixed boundary conditions at the bottom of the domain cannot be satisfied by (3.1) since it has no  $X$  dependence, so an inner solution is needed. It is important to notice that the form of the outer solution is independent of the particular structure of the substrate at  $y = 0$ , the periodicity in  $X$  so far being the only requirement for the outer solution to take the form (3.1).

#### 3.2 Inner region: $y = O(\epsilon)$

The effect of the ridges becomes significant when  $y$  is comparable to the ridge period, i.e.,  $y \sim x = \epsilon X = O(\epsilon)$ , and both terms of the Laplacian balance in (2.1). We introduce  $Y = y/\epsilon$ , which is  $O(1)$  as  $\epsilon \rightarrow 0$  in the inner region. The solution here, denoted  $w = W(X, Y)$ , satisfies

$$\frac{\partial^2 W}{\partial X^2} + \frac{\partial^2 W}{\partial Y^2} = -2\epsilon^2, \quad (3.2)$$

In inner variables  $(X, Y)$ , the conditions at the bottom of the domain are identical to (2.3) and (2.4), with the meniscus occupying  $X \in [-\delta, \delta]$  in a period window  $[-1, 1]$ . Using Van Dyke's matching principle for matching with the outer region,  $W$  as  $Y \rightarrow \infty$  must be identical to (3.1) with  $y = \epsilon Y$  substituted, giving

$$W \sim -\epsilon^2 Y^2 + \epsilon Y + B(\epsilon)(1 - \epsilon Y), \quad \text{as } Y \rightarrow \infty. \quad (3.3)$$

As (3.1) holds to all algebraic orders in  $\epsilon$ , (3.3) must hold to all orders in  $Y$ . It can be shown [Hodes et al., 2017] that  $W = 0$  for  $\epsilon = 0$ , implying  $B(\epsilon) = O(\epsilon)$ , or  $\hat{B}(\epsilon) = B(\epsilon)/\epsilon = O(1)$ .

This inner problem can be reduced to Laplace's equation in a semi-infinite domain, driven by a shear-flow, with the following substitution,

$$W = -\epsilon^2 Y^2 + [1 - \epsilon \hat{B}(\epsilon)] \epsilon \widehat{W}. \quad (3.4)$$

Along with periodicity or symmetry conditions at  $X = \pm 1$ , the problem for  $\widehat{W}$  is given by

$$\frac{\partial^2 \widehat{W}}{\partial X^2} + \frac{\partial^2 \widehat{W}}{\partial Y^2} = 0, \quad (3.5)$$

$$\widehat{W} = 0, \quad \text{on } Y = 0, X \notin [-\delta, \delta] \quad (3.6)$$

$$\mathbf{n} \cdot \nabla_{XY} \widehat{W} = [1 + \epsilon \hat{\lambda}(\epsilon)] \mathbf{n} \cdot \nabla_{XY} (\epsilon Y^2), \quad \text{on the meniscus } S \quad (3.7)$$

$$\widehat{W} \sim Y + \hat{\lambda}(\epsilon), \quad \text{as } Y \rightarrow \infty. \quad (3.8)$$

where  $\hat{\lambda}(\epsilon) = \hat{B}(\epsilon)/(1 - \epsilon \hat{B}(\epsilon)) = O(1)$ , and  $\nabla_{XY} = (\partial/\partial X, \partial/\partial Y)$  is the gradient in the inner coordinates.

We remark that  $\widehat{W}$  is  $O(1)$  but depends on  $\epsilon$ . A formal expansion of  $\widehat{W}$  in  $\epsilon$  is unnecessary, as any solution method at  $O(\epsilon)$  can be used to solve the unexpanded problem directly. The above problem is similar to that considered by Crowdy [2010, 2016] but with an additional nonconstant forcing on the meniscus. This term is not present if the meniscus is flat or if we restrict to leading order ( $\epsilon = 0$ ), in which case  $\widehat{W}$  corresponds exactly to the unbounded shear-flow over the same surface, and  $\hat{\lambda}$  is the associated slip length. For a meniscus shape  $Y(X)$ , the forcing term can be written

$$\mathbf{n} \cdot \nabla_{XY} (\epsilon Y^2) = \frac{2\epsilon Y}{(1 + Y'^2)^{1/2}}, \quad (3.9)$$

where  $Y'(X) = dY/dX$ . If  $Y(X)$  is a circular arc, this is a known function of  $X$ .

Finally, just as in Hodes *et al.*, the solution is the same in the outer region as the overlap region, so a composite solution uniformly valid throughout the entire domain is simply the inner solution:

$$w_{comp} = W = -y^2 + \frac{\epsilon}{1 + \epsilon \hat{\lambda}} \widehat{W}. \quad (3.10)$$

## 4 Solution of inner problem: small slip fraction, $\delta \ll 1$

We make no further approximation in  $\epsilon$ , and to solve the inner problem given by (3.5)-(3.8) we consider the additional limit of small slip fraction,  $\delta = c^*/l^* \ll 1$ , or the dilute limit. The problem Crowdy [2010, 2016] considered corresponds to (3.5)-(3.8) with  $\epsilon = 0$ , a shear-free meniscus. Therefore we present an extension of Crowdy [2016] to account for this inhomogeneity—the full details are given in the Supplementary Material. Since  $\widehat{W}$  is harmonic, let  $\hat{h}(z)$  with  $z = X + iY$  be its complex potential such that  $\widehat{W} = \text{Im}\{\hat{h}(z)\}$ . If the

complex potential for the flow over a single such meniscus is  $\hat{h}_s(z)$ , then repeating Crowdy's superposition arguments gives the first two approximations to the periodic case as:

$$\hat{h}_0(z) = \hat{h}_s(z) + \hat{\lambda}_0 \left[ \frac{2}{\pi z} - \cot \left( \frac{\pi z}{2} \right) \right], \quad \hat{\lambda}_0 = \frac{\lambda_0 - \epsilon \delta^3 I}{1 + \epsilon^2 \delta^3 I}, \quad (4.1)$$

$$\hat{h}_1(z) = \hat{h}_s(z) + \hat{\lambda}_1 \left[ \frac{2}{\pi z} - \cot \left( \frac{\pi z}{2} \right) + \frac{\pi}{6} (h_s(z) - z) \right], \quad \hat{\lambda}_1 = \frac{\lambda_1 - \epsilon \delta^3 (1 + \frac{\pi}{6} \lambda_1) I}{1 + \epsilon^2 \delta^3 (1 + \frac{\pi}{6} \lambda_1) I}, \quad (4.2)$$

where  $\lambda_0$ ,  $\lambda_1$ ,  $I(\theta)$  are (1.1), (1.3), and  $h_s(z)$  is the potential for a single shear-free meniscus. It can be shown that (4.1) and (4.2) satisfy the requirements for  $\hat{h}(z)$  with errors of  $O(\delta^3)$  and  $O(\delta^5)$ , respectively. The potential  $\hat{h}_s(z)$  is found by conformally mapping the flow domain to an auxiliary  $\zeta$ -domain (upper half-disk) via

$$\zeta(z) = \frac{(z/\delta - 1)^{1/\alpha} - (z/\delta + 1)^{1/\alpha}}{(z/\delta - 1)^{1/\alpha} + (z/\delta + 1)^{1/\alpha}}, \quad \alpha = \frac{2}{\pi}(\pi - \theta), \quad (4.3)$$

then analytically continuing to the unit disk and invoking the Poisson integral formula. The result takes the form

$$\hat{h}_s(z(\zeta)) = \frac{\delta}{\alpha} (\zeta - \zeta^{-1}) + \frac{1}{2\pi i} \int_{|\zeta'|=1} \frac{d\zeta' \zeta' + \zeta}{\zeta' \zeta' - \zeta} f(\zeta'), \quad f(\zeta) = \begin{cases} \chi[z(\zeta)] & \text{Im}(\zeta) \geq 0, \\ \chi[z(\zeta^{-1})] & \text{Im}(\zeta) < 0, \end{cases}$$

where  $\chi(z)$  is the real integral  $[1 + \epsilon \hat{\lambda}(\epsilon)] \int^X 2\epsilon Y(X') dX'$  written in terms of  $z = X + iY$ .

## 5 Apparent slip length

The apparent slip length  $\beta$  of a channel flow is defined, following Lauga and Stone [2003], by equating the flow rate per unit width,  $Q$ , with that of an effective Navier slip profile

$$w_{NS} = -y^2 + \frac{y + \beta}{1 + \beta}, \quad Q_{NS} = \frac{1}{2\epsilon} \int_{-\epsilon}^{\epsilon} \int_0^1 w_{NS} dy dx = \frac{2}{3} - \frac{1}{2(1 + \beta)}, \quad (5.1)$$

which satisfies a Navier slip condition  $w_{NS} = \beta dw_{NS}/dy$  at  $y = 0$ , and  $w_{NS} = 0$  at  $y = 1$ . The outer solution (3.1), written in terms of  $\hat{\lambda}$ , already takes the form of a Navier slip profile:

$$w = -y^2 + \frac{y + \epsilon \hat{\lambda}}{1 + \epsilon \hat{\lambda}}. \quad (5.2)$$

However, this does not imply that  $\epsilon \hat{\lambda}$  is our approximation to  $\beta$ , since the flow rate  $Q = \frac{1}{2\epsilon} \int_D w(x, y) dx dy$  will have contributions from the inner region. The effective Navier slip profile must be integrated over a rectangular cross-section, but the actual flow cross-section is not rectangular when the meniscus is curved. This difference in cross-section complicates the relationship between  $\beta$  and  $\epsilon \hat{\lambda}$ , and there is a contribution from the change in area.

To calculate  $Q$  we derive a reciprocal result from Green's second identity in the cross-section  $D$  with  $\frac{1}{2}y^2$  and  $w(x, y)$  (which satisfies (2.1)-(2.4)) as the chosen functions. The identity states that

$$\int_D \left[ w \nabla^2 \left( \frac{1}{2} y^2 \right) - \frac{1}{2} y^2 \nabla^2 w \right] dA = - \int_{\partial D} \left[ w \frac{\partial}{\partial n} \left( \frac{1}{2} y^2 \right) - \frac{1}{2} y^2 \frac{\partial w}{\partial n} \right] ds, \quad (5.3)$$

where  $\partial/\partial n$  is the inward normal derivative. Now,  $\nabla^2 w = -2$ ,  $\nabla^2(y^2/2) = 1$ , and the only surviving boundary integrals are along  $y = 1$  and the meniscus,

$$\int_D w dA + \int_D y^2 dA = \int_{y=1} -\frac{1}{2} \frac{\partial w}{\partial y} dx - \int_S w \frac{\partial}{\partial n} \left( \frac{1}{2} y^2 \right) ds. \quad (5.4)$$

Substituting the outer solution at  $y = 1$ , the inner solution on the meniscus, and rearranging,

$$2\epsilon Q = - \int_D y^2 dA + 2\epsilon \left[ 1 - \frac{1}{2(1 + \epsilon \hat{\lambda})} \right] + \int_S y^3 \frac{\partial y}{\partial n} ds - \frac{\epsilon}{1 + \epsilon \hat{\lambda}} \int_S \widehat{W} y \frac{\partial y}{\partial n} ds. \quad (5.5)$$

Each integral is straightforwardly evaluated from the geometry except the last, which requires the inner solution on the meniscus. Using the approximation (4.2), and neglecting terms of  $O(\delta^7)$ , this becomes  $Q = Q_{outer} + Q'$  where  $Q_{outer}$  is the flow rate of the outer slip profile down to  $y = 0$ , and  $Q'$  the extra contribution from the change in shape,

$$Q_{outer} = \frac{2}{3} - \frac{1}{2(1 + \epsilon \hat{\lambda})}, \quad Q' = -\frac{\epsilon^2 \delta^3}{2(1 + \epsilon \hat{\lambda})} I(\theta) + \frac{1}{2} \epsilon^3 \delta^4 [F(\theta) - G(\theta)] + O(\delta^7), \quad (5.6)$$

where  $I(\theta)$ ,  $F(\theta)$  are (1.3), (1.4). Then  $G(\theta)$  is given by the integral

$$G(\theta) = \int_0^\pi d\phi K(\phi; \theta) \int_{-\pi}^\pi \frac{d\psi}{2\pi} \cot \left( \frac{\phi - \psi}{2} \right) g(\psi; \theta), \quad (5.7)$$

$$K(\phi; \theta) = 4\alpha \sin \theta \frac{\tan^{2\alpha}(\phi/2) [\cos \theta + 2 \tan^\alpha(\phi/2) + \cos \theta \tan^{2\alpha}(\phi/2)]}{\sin \phi [1 + 2 \cos \theta \tan^\alpha(\phi/2) + \tan^{2\alpha}(\phi/2)]^3}, \quad (5.8)$$

$$g(\psi; \theta) = \csc^2 \theta \operatorname{ilog} \left[ i \frac{e^{i\theta/2} + e^{-i\theta/2} \tan^\alpha(|\psi|/2)}{e^{-i\theta/2} + e^{i\theta/2} \tan^\alpha(|\psi|/2)} \right] \quad (5.9)$$

$$+ \csc \theta \frac{[1 - \tan^{2\alpha}(|\psi|/2)] [\cos \theta + 2 \cos 2\theta \tan^\alpha(|\psi|/2) + \cos \theta \tan^{2\alpha}(|\psi|/2)]}{[1 + 2 \cos \theta \tan^\alpha(|\psi|/2) + \tan^{2\alpha}(|\psi|/2)]^2}, \quad (5.10)$$

or by the correlation (accurate to within 0.2% on  $[-\pi/2, \pi/2]$ ),

$$G(\theta) \approx -0.4574 \theta^2 + 0.08568 \theta^3 - 0.1654 \theta^4 + 0.01413 \theta^5 - 0.01714 \theta^6 + 0.01450 \theta^7 - 0.01917 \theta^8. \quad (5.11)$$

Finally, equating  $Q$  with (5.1), and using the  $\hat{\lambda}_1$  approximation for  $\hat{\lambda}$ , we arrive at the formula (1.2) for the slip length  $\beta$ . The corresponding formula for a channel with ridges on



$\delta$	$\epsilon$			
	0.01	0.1	0.5	2.5
0.1	0.17	0.099	0.087	1.2
0.25	0.025	0.029	0.031	6.8
0.5	0.83	0.83	0.83	-
0.75	6.3	6.3	7.8	-

Table 1: Maximum relative error (%) of  $\beta/(2\epsilon\delta^2)$  over  $-\pi/2 \leq \theta \leq \pi/2$ , between formula (1.2) and numerical solution. For  $\epsilon = 2.5$ ,  $\delta = 0.5, 0.75$  see figure 5.2.

both walls—see Supplementary Material—is (1.5), and it involves all the same quantities. These explicit formulas (1.2), (1.5) are the main results of the paper. Each function of  $\theta$  appearing in (1.2) is smooth, regular, and easily computed. Even  $G(\theta)$ , which comes from the velocity on the meniscus, is accurately computed using the trapezoidal rule and skipping the singular point of the cotangent.

The quantity  $Q'$  can be roughly interpreted as the change in flow rate due to the change in cross-sectional shape and area due to meniscus protrusion, i.e., a generalisation of  $Q_2^{(1)}$  in [Sbragaglia and Prosperetti, 2007] to arbitrary  $\theta$ . From (5.6), we see that  $Q' = O(\epsilon^2)$ , thus its contribution is necessary to compute  $\beta$  beyond leading order in  $\epsilon$ . This differs greatly from the case of a flat meniscus, where  $Q' \equiv 0$  and (1.2) reduces to  $\beta = \epsilon\lambda$  to all orders in  $\epsilon$  [Hodes et al., 2017].

Two distinct asymptotic approximations,  $\epsilon \ll 1$  and  $\delta \ll 1$ , were made in order to derive (1.2). All algebraic orders in  $\epsilon$  were accounted for before the dilute limit  $\delta \ll 1$  was taken, but only up to  $O(\delta^5)$ , and thus the accuracy is limited by that of the  $\delta$ -expansion. This is apparent when compared against finite-element computations of the full problem in the literature. Figure 5.1 compares  $\beta/(2\epsilon\delta^2)$  using formula (1.2) for ridges on one wall with results using PDEToolbox in Matlab (see Karamanis et al. [2017]), for the same parameters as Teo and Khoo [2010]. The accuracy is uniform for the whole range of  $\theta \in [-\pi/2, \pi/2]$ , and the maximum relative errors are shown in table 1. The accuracy in  $\epsilon$  is remarkable, a negligible change is seen up to  $\epsilon = 0.5$ , when the channel height equals the period. Even more remarkable is that the error is still only 2 – 6% up to  $\epsilon = 2.5$ , when the height is five times *smaller* than the period. For this case, at slip fractions  $\delta = 0.5, 0.75$ , the height is low enough for the slip length to become negative, which the asymptotics capture excellently, and for the meniscus to make contact with the upper wall; this occurs at  $\theta = 77^\circ, 56^\circ$  for  $\delta = 0.5, 0.75$ , see figure 5.2. However, for these parameters, the slip length becomes singular for sufficient downward protrusion ( $\theta < 0$ ), due to a breakdown of the slip length definition (5.1), which rearranged is  $\beta = 1/(4/3 - 2Q) - 1$ . This is singular when  $Q = 2/3$ , the flow rate for complete slip, i.e.,  $\partial w/\partial y = 0$  on  $y = 0$ . For flow rates above  $2/3$ , the enhancement due to the increase in area is greater than even complete slip, and  $\beta$  loses its physical interpretation. This was not seen by Teo and Khoo [2010] or Sbragaglia and Prosperetti [2007] as they seem to use a definition for  $\beta$  that is only valid for small  $\beta$ . If we directly consider the flow rate enhancement relative to no-slip Poiseuille flow,  $\Delta Q = Q - 1/6$ , there is no singularity—see

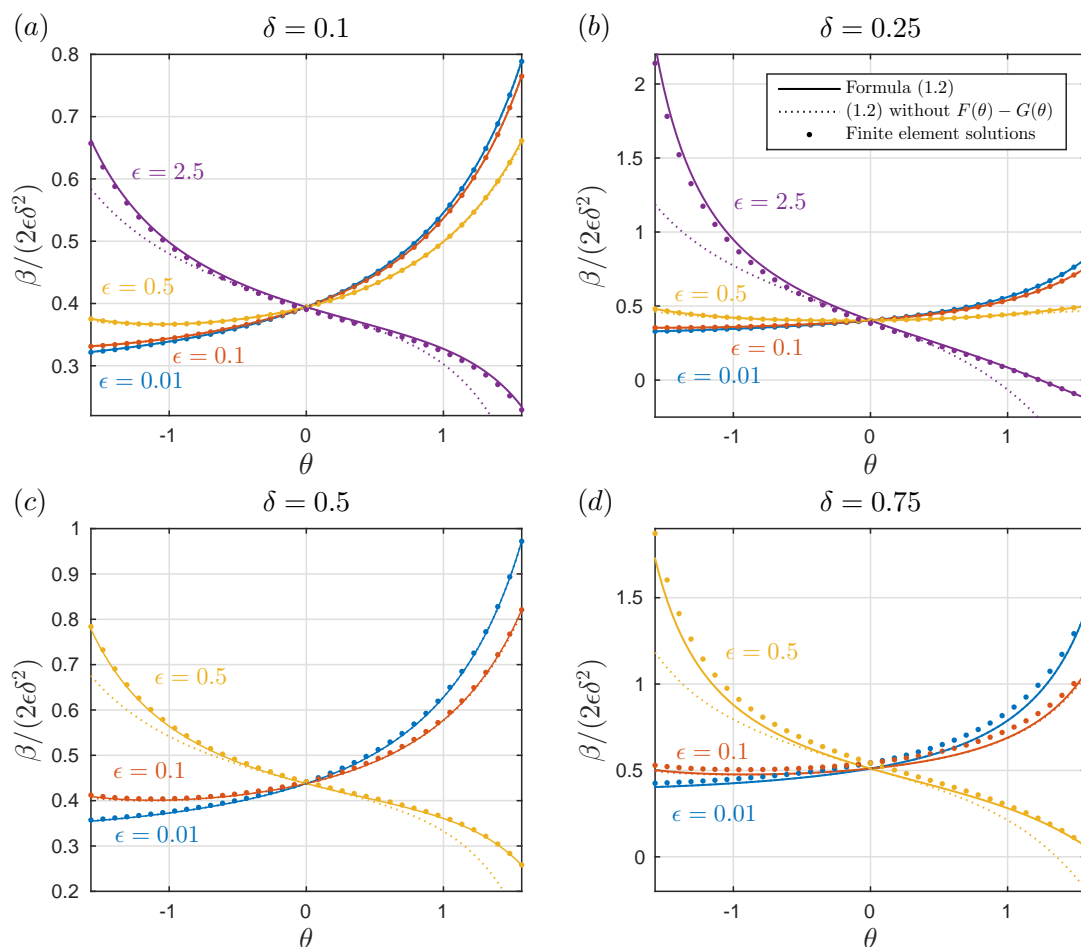


Figure 5.1: Normalised slip length against protrusion angle for slip fractions  $\delta = 0.1, 0.25, 0.5, 0.75$  and various aspect ratios  $\epsilon$ . Solid lines are the full asymptotic solution (1.2); dotted lines are (1.2) with  $F$  and  $G$  neglected; dots are finite-element solutions.

figure 5.2(b)—and the maximum relative error of the asymptotics is 5 – 8%.

Further simplifications of the formula (1.2) are possible, but the accuracy can be greatly affected with little analytical gain. For example, if the  $F(\theta)$  and  $G(\theta)$  terms are neglected in (1.2), the formula is simpler but the accuracy for large angles is much worse—see dotted lines in figures 5.1 and 5.2. Other simplifications, such as using the lower order approximations  $\hat{h}_0(z)$  and  $\hat{\lambda}_0$  in (5.5), or expanding fractional terms, are even less accurate still, thus we do not include them here.

This work was supported by an EPSRC Doctoral Scholarship and Doctoral Prize Fellowship. The author is grateful to Darren Crowdy for many helpful discussions and the inspiration for section 4, and to Georgios Karamanis for the finite element data.

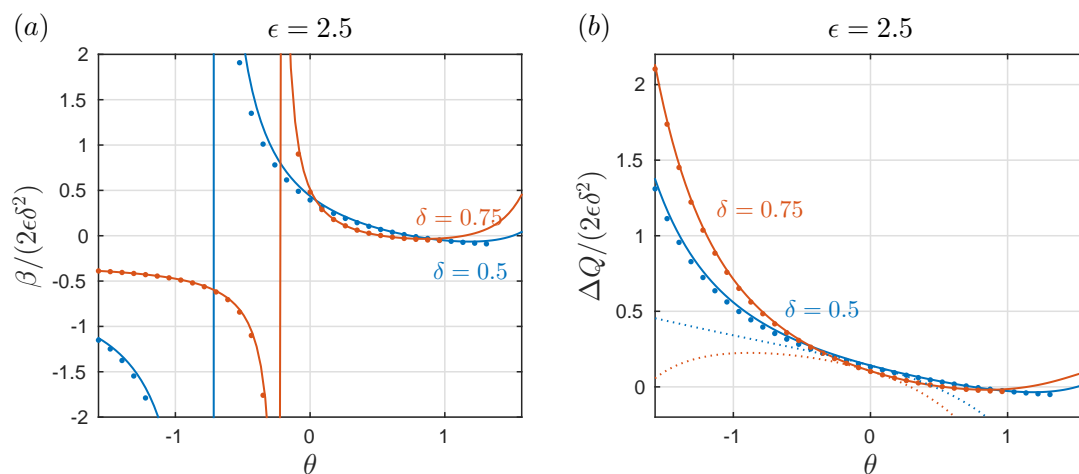


Figure 5.2: Normalised slip length and change in flow rate against protrusion angle for slip fractions  $\delta = 0.5, 0.75$  and at  $\epsilon = 2.5$ . Solid lines are the full asymptotic solution (1.2) and (5.6); dotted lines in (b) are (1.2) with  $F$  and  $G$  neglected; dots are finite element solutions.

## References

- C. Cottin-Bizonne, C. Barentin, E. Charlaix, L. Bocquet, and J. L. Barrat. Dynamics of simple liquids at heterogeneous surfaces: Molecular-dynamics simulations and hydrodynamic description. *Eur. Phys. J. E*, 15(4):427–438, 2004. ISSN 1292-8941. doi: 10.1140/epje/i2004-10061-9.
- D. G. Crowdy. Slip length for longitudinal shear flow over a dilute periodic mattress of protruding bubbles. *Phys. Fluids*, 22(12):121703, 2010. ISSN 1070-6631. doi: 10.1063/1.3531683.
- D. G. Crowdy. Analytical formulae for longitudinal slip lengths over unidirectional superhydrophobic surfaces with curved menisci. *J. Fluid Mech.*, 791:R7, 2016. ISSN 1469-7645. doi: 10.1017/jfm.2016.88.
- J. Davies, D. Maynes, B. W. Webb, and B. Woolford. Laminar flow in a microchannel with superhydrophobic walls exhibiting transverse ribs. *Phys. Fluids*, 18(8):087110, 2006.
- A. M. J. Davis and E. Lauga. Geometric transition in friction for flow over a bubble mattress. *Phys. Fluids*, 21(1):011701, 2009. ISSN 1070-6631. doi: 10.1063/1.3067833.
- R. Enright, M. Hodes, T. Salamon, and Y. Muzychka. Isoflux Nusselt number and slip length formulae for superhydrophobic microchannels. *J. Heat Trans-T ASME*, 136(1):012402, 2014.
- M. Hodes, T. L. Kirk, G. Karamanis, and S. MacLachlan. Effect of thermocapillary stress on slip length for a channel textured with parallel ridges. *J. Fluid Mech.*, 814:301–324, 2017.

- G. Karamanis, M. Hodes, T. Kirk, and D. Papageorgiou. Solution of the Graetz–Nusselt problem for liquid flow over isothermal parallel ridges. *J. Heat Trans-T ASME*, 139(9):091702, 2017.
- T. L. Kirk, M. Hodes, and D. T. Papageorgiou. Nusselt numbers for Poiseuille flow over isoflux parallel ridges accounting for meniscus curvature. *J. Fluid Mech.*, 811:315–349, 2017.
- L. S. Lam, M. Hodes, and R. Enright. Analysis of Galinstan-based microgap cooling enhancement using structured surfaces. *J. Heat Trans-T ASME*, 137(9):091003, 2015. ISSN 0022-1481. doi: 10.1115/1.4030208.
- E. Lauga and H. A. Stone. Effective slip in pressure-driven Stokes flow. *J. Fluid Mech.*, 489:55–77, 2003.
- D. Maynes and J. Crockett. Apparent temperature jump and thermal transport in channels with streamwise rib and cavity featured superhydrophobic walls at constant heat flux. *J. Heat Trans-T ASME*, 136(1):011701, 2014. ISSN 0022-1481. doi: 10.1115/1.4025045.
- D. Maynes, B. W. Webb, and J. Davies. Thermal transport in a microchannel exhibiting ultrahydrophobic microribs maintained at constant temperature. *J. Heat Trans-T ASME*, 130(2):022402, 2008. ISSN 0022-1481. doi: 10.1115/1.2789715.
- D. Maynes, B. W. Webb, J. Crockett, and V. Solovjov. Analysis of laminar slip-flow thermal transport in microchannels with transverse rib and cavity structured superhydrophobic walls at constant heat flux. *J. Heat Trans-T ASME*, 135(2):021701, 2013. ISSN 0022-1481. doi: 10.1115/1.4007429.
- C.-O. Ng and C. Y. Wang. Effective slip for Stokes flow over a surface patterned with two- or three-dimensional protrusions. *Fluid Dyn. Res.*, 43(6):065504, 2011.
- J. Ou and J. P. Rothstein. Direct velocity measurements of the flow past drag-reducing ultrahydrophobic surfaces. *Phys. Fluids*, 17(10):103606, 2005. ISSN 1070-6631. doi: 10.1063/1.2109867.
- J. Ou, B. Perot, and J. P. Rothstein. Laminar drag reduction in microchannels using ultrahydrophobic surfaces. *Phys. Fluids*, 16(12):4635–4643, 2004.
- M. Sbragaglia and A. Prosperetti. A note on the effective slip properties for microchannel flows with ultrahydrophobic surfaces. *Phys. Fluids*, 19(4):043603, 2007. ISSN 1070-6631. doi: 10.1063/1.2716438.
- O. Schnitzer. Slip length for longitudinal shear flow over an arbitrary-protrusion-angle bubble mattress: the small-solid-fraction singularity. *J. Fluid Mech.*, 820:580–603, 2017. doi: 10.1103/PhysRevFluids.1.052101.

- A. Steinberger, C. Cottin-Bizonne, P. Kleimann, and E. Charlaix. High friction on a bubble mattress. *Nat. Mater.*, 6(9):665–668, 2007. ISSN 1476-1122. doi: {10.1038/nmat1962}.
- C. J. Teo and B. C. Khoo. Analysis of Stokes flow in microchannels with superhydrophobic surfaces containing a periodic array of micro-grooves. *Microfluid. Nanofluid.*, 7(3):353–382, 2009. ISSN 1613-4982. doi: 10.1007/s10404-008-0387-0.
- C. J. Teo and B. C. Khoo. Flow past superhydrophobic surfaces containing longitudinal grooves: effects of interface curvature. *Microfluid. Nanofluid.*, 9(2-3):499–511, 2010. ISSN 1613-4982. doi: 10.1007/s10404-010-0566-7.
- L. P. Wang, C. J. Teo, and B. C. Khoo. Effects of interface deformation on flow through micro-tubes containing superhydrophobic surfaces with longitudinal ribs and grooves. *Microfluid. Nanofluid.*, 16(1-2):225–236, 2014. ISSN 1613-4982. doi: {10.1007/s10404-013-1201-1}.
- C. Ybert, C. Barentin, C. Cottin-Bizonne, P. Joseph, and L. Bocquet. Achieving large slip with superhydrophobic surfaces: Scaling laws for generic geometries. *Phys. Fluids*, 19(12): 123601, 2007. doi: 10.1063/1.2815730.